BIOCHEMISTRY
including biophysical chemistry & molecular biology

Article

pubs.acs.org/biochemistry

# Toward an Understanding of Agonist Binding to Human Orexin-1 and Orexin-2 Receptors with G-Protein-Coupled Receptor Modeling and Site-Directed Mutagenesis

Alexander Heifetz,*[,†] Oliver Barker,[†] G. Benjamin Morris,[§] Richard J. Law,[†] Mark Slack,[‡] and Philip C. Biggin*[,§]

[†]Evotec (U.K.) Ltd., 114 Innovation Drive, Milton Park, Abingdon, Oxfordshire OX14 4RZ, U.K.

[‡]Evotec AG, Manfred Eigen Campus, Essener Bogen 7, 22419 Hamburg, Germany

[§]Department of Biochemistry, University of Oxford, South Parks Road, Oxford OX1 3QU, U.K.

Supporting Information

**ABSTRACT:** The class A G-protein-coupled receptors (GPCRs) Orexin-1 (OX1) and Orexin-2 (OX2) are located predominantly in the brain and are linked to a range of different physiological functions, including the control of feeding, energy metabolism, modulation of neuro-endocrine function, and regulation of the sleep−wake cycle. The natural agonists for OX1 and OX2 are two neuropeptides, Orexin-A and Orexin-B, which have activity at both receptors. Site-directed mutagenesis (SDM) has been reported on both the receptors and the peptides and has provided important insight into key features responsible for agonist activity. However, the structural interpretation of how these data are linked together is still lacking. In this work, we produced and used SDM data, homology modeling followed by MD simulation, and ensemble-flexible docking to generate binding poses of the Orexin peptides in the OX receptors to rationalize the SDM data. We also developed a protein pairwise similarity comparing method (ProS) and a GPCR-likeness assessment score (GLAS) to explore the structural data generated within a molecular dynamics simulation and to help distinguish between different GPCR substates. The results demonstrate how these newly developed methods of structural assessment for GPCRs can be used to provide a working model of neuropeptide−Orexin receptor interaction.

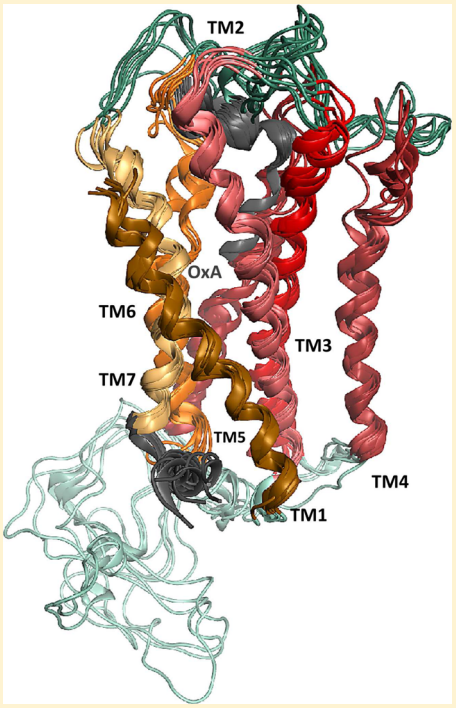


The class A G-protein-coupled receptors Orexin-1 (OX1) and Orexin-2 (OX2) are located predominantly in the hypothalamus and locus coeruleus[1,2] but are also found elsewhere in the central nervous system.[3,4] The Orexin (OX) receptors are highly conserved across mammalian species. The human (h) OX1 and OX2 receptors have 64% identical overall sequences, being 84% identical in the transmembrane regions. The sequence alignment of hOX1 and hOX2 is shown in Figure 1. The OX receptors are linked to a range of different physiological functions, including the control of feeding, energy metabolism, modulation of neuroendocrine function,[5,6] and regulation of the sleep−wake cycle.[7,8] They are also associated with dopaminergic neurons of the ventral tegmental area (VTA)[9] that are critical elements of the reward system.[10] Although the hypothalamic OX system is known to regulate appetitive behaviors[11,12] and promote wakefulness and arousal,[13] this system may also be important in adaptive and pathological anxiety/stress responses.[14−16]

Over the past decade, a large number of OX antagonists have been developed as potential drugs for various physiological disorders involving the Orexin system. Currently, the most clinically advanced Orexin antagonist is Suvorexant[17] for the treatment of insomnia. However, it is not only OX antagonists that have therapeutic potential;[15,18] it has also been shown that agonists of OX receptors have potential[18−20] for the treatment of various diseases, including narcolepsy, obesity, hypophagia, attention deficit hyperactivity disorder,[18] bipolar disorders, Parkinson's disease,[21] and colon cancer.[22] By extension,

**Received:** August 16, 2013
**Revised:** October 21, 2013
**Published:** October 21, 2013

  

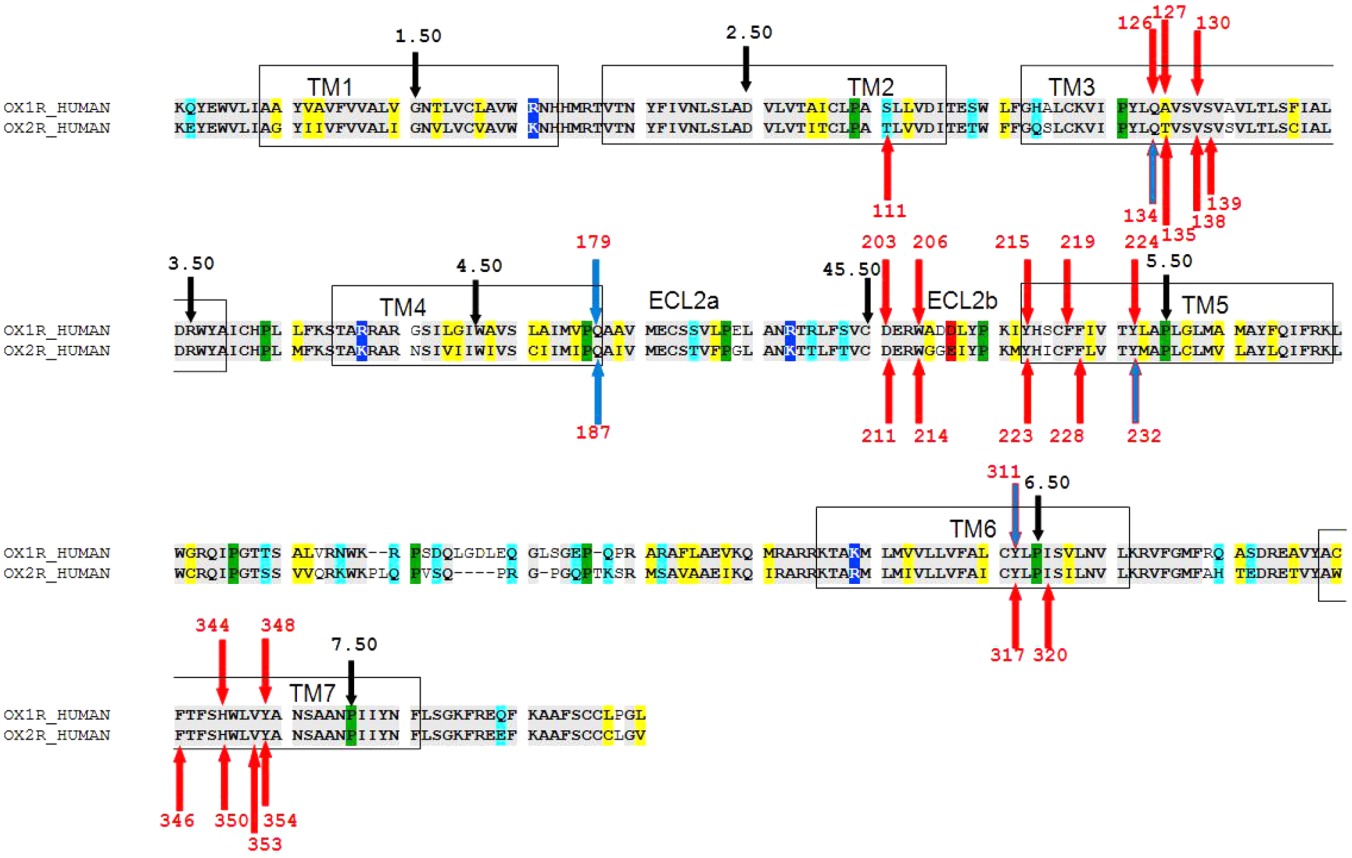


**Figure 1.** Sequence alignment of hOX1 (OX1R_HUMAN) and hOX2 (OX2R_HUMAN). The background color coding is as follows: gray for identical residues, yellow for chemically homologous residues, cyan for polar residues, blue for positive residues, red for negative residues, and green for prolines. The key residues that were involved in SDM are shown by colored arrows: red arrows for residues mutated by other researchers, blue arrows for mutations introduced by us, and blue arrows with a red outline for mutations introduced by other researchers and by us. The conserved residue in each TM that is assigned to 50 according to the Ballesteros–Weinstein numbering scheme is denoted with a black arrow. The red numbers are the amino acid numbers as they are appear in sequences of OX1 (O43613) and human OX2 (O43614), which were retrieved from the Swiss-Prot database.

understanding OX receptor agonist binding is also important for developing inverse agonists or antagonists that block this activity. Moreover, the study of OX agonists is especially important in light of "biased signaling" of GPCR ligands[23] and the recent discovery that OX receptors can also signal via the $\beta$2-arrestin signaling pathway.[24] This observation is particularly important because many of the antagonists originally thought to block one signaling pathway have a second "hidden" activity as agonists of second signaling pathways, as was shown for the antagonists of human H4.[25] Thus, in light of the broad medicinal evidence of the importance of OX receptors as potential drug targets,[7,26,27] there is a need for the exploration of the key structural features of OX receptors involved in agonist potency, efficacy, and selectivity. Such information is vital for driving the development of the first OX receptor nonpeptidic agonists[28,29] or even for improving antagonist performance.[7,30]

It was discovered that hypothalamic neuropeptides Orexin-A/hypocretin-1 [OxA, 33 amino acids (see Figure 2A)][31] and Orexin-B/hypocretin-2 [OxB, 28 amino acids (see Figure 2A)][32] agonize their effect through OX1 and OX2 receptors that couple to $G_{q/11}$ and contribute to the activation of phospholipase C, leading to the elevation of intracellular $Ca^{2+}$ concentrations.[33] The Orexin peptides can be divided into two small "domains", the N-terminus (residues 1–14 in OxA and 1–9 in OxB) and the C-terminus [residues 15–33 in OxA and 10–28 in OxB (see Figure 2A)]. In spite of the functional homology, the Orexin peptides share similarity (79%) only in the C-terminal domain. The N-terminus of OxA contains two intramolecular disulfide bonds formed between C6 and C12 and between C7 and C14. The C-termini of the Orexins are comprised of two consensus $\alpha$-helices[34] connected by a short loop that generates a kink between them.

Recently, several site-directed mutagenesis[35−37] studies were conducted to reveal the key residues in both Orexin receptors (Table 1) and the peptide (Table 2) responsible for their mutual potency and efficacy. Key residues of OxA and OxB required for their binding to the OX1 and OX2 receptors have been explored using truncated peptides and alanine scan approaches, in which each of the peptide residues was systematically substituted with alanine[36,38] or in the case of alanine with glycine. It was observed[38] that deletion of the N-terminal domain produces a decrease in the efficacy of OxA to OX1; however, a C-terminus alone retains a significant agonist effect.[35,38] The biological activity of the mutated peptides was estimated from the transient mobilization of the intracellular calcium concentration, which was mediated by the receptors bound to wild type and mutated peptides.

It was observed[36,38] (Table 2) that mutations of the residues in the truncated C-terminus of OxA (L20A, A27A, A28G, G29A, I30A, L31A, T32A, and L33A) significantly reduce peptide potency with respect to both OX1 and OX2 receptors.


dx.doi.org/10.1021/bi401119m | *Biochemistry* 2013, 52, 8246−8260

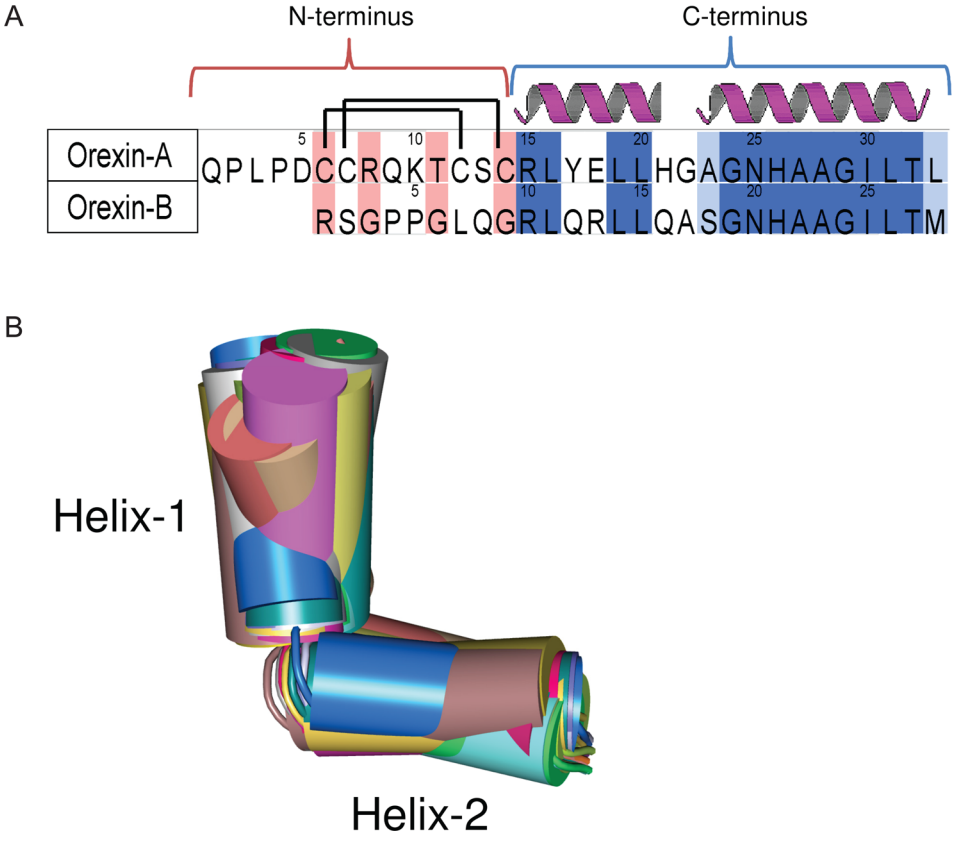


**Figure 2.** (A) Amino acid sequence alignment of human Orexin-A with human Orexin-B, which was retrieved from the Swiss-Prot database (entry O43612). The background color coding is as follows: dark blue for identical residues, light blue for chemically homologous residues, and pink for chemically nonhomologous residues. Two intramolecular disulfide bonds in Orexin-A formed between C6 and C12 and between C7 and C14 are shown as lines. Consensus helical structures[34] are marked with red dashed line. (B) Thirty conformations of the C-terminus truncated from OxA structures determined by NMR and extracted from PDB entry 1WSO.[34] The helical domains are represented by cylinders and loops by tubes. The structures are colored randomly accordingly to their number in the PDB entry.

It was also suggested that the G29A mutation caused a significant disruption of the secondary structure, resulting in a marked decrease in activity. Mutation of L16 and L19 to alanine resulted in a decrease in potency with respect to OX1 but had no effect on OX2. Mutation of H26 to alanine caused a decrease in potency, which was more pronounced for OX1 than for OX2. Other residues of OxA had a negligible effect on potencies with respect to both receptors.

For the truncated C-terminus of OxB, mutations at positions analogous to those of OxA (L15A, N20A, G24A, I25A, L26A, T27A, and M28A) (L33 in OxA) significantly reduce peptide potency with respect to both OX1 and OX2 receptors. Mutations L11A and A22G resulted in a decrease in potency with respect to OX1 but had no effect on that with respect to OX2. Mutation of A23 to glycine caused a decrease in potency, which was more pronounced for OX1 than for OX2. Mutation of the conserved R10 to alanine resulted in a decrease in the potency of OxB with respect to both OX1 and OX2 receptors. Interestingly, the same mutation of (conserved) residue R15 in OxA could be tolerated by both receptors. Mutation of the nonconserved S18 to alanine resulted in a decrease in the potency to OX2 but had no effect on OX1. Mutation of G19 to alanine caused significant disruption to the secondary structure, resulting in a decrease in potency with respect to both OX receptors. Other residues of OxB had a negligible effect on potencies with respect to both receptors.

The receptors themselves have also been the subject of SDM studies with 29 point mutations (18 in hOX2 and 11 in hOX1) that were introduced into the 7TMD region to explore their effect on hOX1 or hOX2 mediation of the Orexin-A-evoked $[Ca^{2+}]_i$ response (see Figure 1 and Table 1).[37]

In OX1, mutations V130A$^{3.36}$, D203A$^{45.51}$, W206A$^{45.54}$, Y215A$^{5.38}$, F219A$^{5.42}$, Y224A$^{5.47}$, Y311A$^{6.48}$, and H344A$^{7.39}$ caused large decreases in the potency of OxA (30.6-, 408.2-, 417.8-, 407.8-, 139.6-, 84.4-, 163.9-, and 241.1-fold, respectively) compared with that of the WT (Table 1). Mutations W206A$^{45.54}$ and Y311A$^{6.48}$ also resulted in decreases in the maximal efficacy ($E_{max}$) of 45.0 and 53.4%, respectively, for OxA and OxB. Other mutations had no major effect on efficacy.

In OX2, mutations T111A$^{2.61}$, D211A$^{45.51}$, W214A$^{5.54}$, Y223A$^{5.38}$, F227A$^{5.42}$, F346A$^{7.35}$, and H350A$^{7.39}$ caused large decreases in the potency of OxA (243.5-, 416.1-, 62.4-, 183.9-, 240.3-, 54.5-, and 49.5-fold, respectively) without affecting their efficacy compared with that of the WT. Mutations Y232A$^{5.47}$ and Y317A$^{6.48}$ resulted in a decrease in both $EC_{50}$ (by 28.4- and 17.7-fold, respectively) and $E_{max}$ (44.9 and 49.6%, respectively) of OxA. Mutation Q134A$^{3.32}$ caused a moderate decrease in the potency of OxA (22.3-fold) without affecting its efficacy.

This SDM data suggests that there is no clear correlation between the importance of residues for potency and for efficacy; residues in positions (Ballesteros and Weinstein[39] numbering) 2.61, 45.51, 5.54, 5.38, 5.42, 7.35, and 7.39 are important for the potency of OxA in both receptors, while


dx.doi.org/10.1021/bi401119m | *Biochemistry* 2013, 52, 8246−8260

**Table 1. Comparison of the Effects of Different Mutations in hOX1 and hOX2 on the Binding Potencies of Orexin-A and Orexin-B[a]**

| | hOX1 | | | hOX2 | | |
|---|---|---|---|---|---|---|
| 7TM position | mutation | ratio[b] of Orexin-A | ratio[b] of Orexin-B | mutation | ratio[b] of Orexin-A | ratio[b] of Orexin-B |
| 2.61 | S103A | NM[f] | | T111A | **243.5**[c] | |
| 3.32 | Q126A | 2.4[c] | | Q134A | **22.3**[c]/**15.1**[d] | 5.1[d] |
| 3.33 | A127T | 1.8[c] | | T135A | 0.8[c] | |
| 3.36 | V130A | **30.6**[c] | | V138A | 4.4[c] | |
| 3.37 | | | | S139A | 2.5[c] | |
| 45.51 | D203A | **408.2**[c] | | D211A | **416.1**[c] | |
| 45.54 | W206A | **417.8**[c] | | W214A | **62.4**[c] | |
| 4.60 | Q179A | **17.8**[d] fold improvement | **72.2**[d] fold improvement | Q187A | 1.3[d] | 1.7[d] |
| 5.38 | Y215A | **407.8**[c] | | Y223A | **183.9**[c] | |
| 5.42 | F219A | **139.6**[c] | | F227A | **240.3**[c] | |
| 5.42 | | | | F227W | **84.2**[d] | **75.0**[d] |
| 5.43 | | | | F228A | 3.0[c] | |
| 5.47 | Y224A | **84.4**[c] | | Y232A | **28.4**[c] | |
| 6.48 | Y311A | **163.9**[c]/ **ND**[e] | **ND**[e] | Y317A | **17.7**[c] | |
| 6.48 | Y311F | 1.6[d] | 0.85[d] | Y317F | 1.3[c] | |
| 6.51 | | | | I320A | 0.9[c] | |
| 7.35 | | | | F346A | **54.5**[c] | |
| 7.39 | H344A | **241.1**[c] | | H350A | **49.5**[c] | |
| 7.42 | | | | V353A | 1.9[c] | |
| 7.43 | Y348A | 8.7[c] | | Y354A | 3.7[c] | |

[a]Determination of the effect of point mutations on the potencies of OX endogenous agonists relative (ratio) to the wild type. The mutations that have a large (≥10-fold) effect are shown in bold. [b]$EC_{50}$(mut)/$EC_{50}$(WT). [c]SDM data generated by Malherbe et al.[37] [d]SDM data generated in this work. [e]No activity detected. [f]Not measured

**Table 2. Effect of Alanine Scanning on the Potencies of Truncated OxA and OxB with Respect to hOX1 and hOX2[a]**

| | | OX1 | | OX2 | |
|---|---|---|---|---|---|
| OxA residue | OxB residue | OxA[34,38] | OxB[36] | OxA[35] | OxB[36] |
| **R15** | **R10** | = | ↓ | = | ↓ |
| **L16** | **L11** | ↓ | ↓ (L11S ↓↓↓) | = | = |
| Y17 | Q12 | = | = | = | = |
| E18 | R13 | = | = | = | = |
| **L19** | **L14** | ↓↓ | = | = | = |
| **L20** | **L15** | ↓↓ | ↓↓ | ↓↓ | ↓↓ |
| H21 | Q16 | = | = | = | = |
| G22 | A17 | = | = | = | = |
| A23 | S18 | = | = | NM[b] | ↓↓ |
| **G24** | **G19** | = | ↓ | = | ↓ |
| **N25** | **N20** | = | ↓↓ | = | ↓↓ |
| **H26** | **H21** | ↓↓ | = | ↓ | = |
| **A27G** | **A22G** | ↓↓ | ↓ | ↓↓ | = |
| **A28G** | **A23G** | ↓↓ | ↓↓ | ↓↓ | ↓ |
| **G29** | **G24** | ↓↓↓ | ↓↓↓ | ↓↓↓ | ↓↓↓ |
| **I30** | **I25** | ↓↓↓ | ↓↓↓ | ↓↓↓ | ↓↓↓ |
| **L31** | **L26** | ↓↓↓ | ↓↓↓ | ↓↓↓ | ↓↓↓ |
| **T32** | **T27** | ↓↓↓ | ↓↓↓ | ↓↓↓ | ↓↓↓ |
| L33 | M28 | ↓↓↓ | ↓↓↓ | ↓↓↓ | ↓↓↓ |

[a]Notations: =, the same potency as the wild type (mutated/wt ratio of <10-fold); ↓↓↓, no binding potency (mutated/wt ratio of >100-fold); ↓↓, statistically significant decrease in binding potency (mutated/wt ratio of ≥20-fold); ↓, statistically moderate decrease in potency (mutated/wt ratio of ≤10−20-fold). Identical residues are shown in bold. [b]Not measured.

mutations at other positions (45.45 and 6.48 in OX1 and 5.47 and 6.48 in OX2) reduce both potency and efficacy.

In this work, we used SDM data, OxA NMR structures, OxB models, and OX1 and OX2 models to explain the role of key residues in both peptides and receptors responsible for agonist binding. We used homology modeling followed by MD simulation and ensemble-flexible docking to generate docking poses of Orexins in the inactive or semiactive forms of the OX receptors. We flexibly docked the Orexin peptides into post-MD substates of inactive forms of Orexin receptors. A significant body of evidence suggests that GPCRs are not simple two-state switches but rather encompass a wide spectrum of states, substates and intermediates.[40] It has been observed that GPCRs exist in at least two highly populated distinct inactive states and in many intermediate substates.[40] Furthermore, recently published NMR data suggest that there is a dynamic equilibrium between functional substates[40] of GPCRs and that agonists initially bind to the inactive state of the GPCR and then promote it toward the active state. Ligands play a key role in stabilizing or destabilizing intermediates involved in GPCR activation and have a clear influence on GPCR substate populations. In simplistic terms, a positive enthalpy change upon activation often reflects the loss of stabilizing interhelical interactions associated with the inactive state, while increases in entropy can be associated with increased protein dynamics[41] or the release of waters of hydration.[42] The addition of an agonist increases the relative population of the activation intermediates for a sufficient period of time to engage a G-protein.[40] Dynamic computational techniques such as MD simulations followed by flexible docking have the potential to go beyond the use of static homology models.[43−51] They offer a way to sample different functional substates of the GPCRs[40,52,53] and for the rationalization of its ligand binding and functional effects.[39,54−60] However, when using this approach, one is often unsure of the relevance of all the substates sampled. To help prioritize the analysis of the


dx.doi.org/10.1021/bi401119m | Biochemistry 2013, 52, 8246−8260

sampled substates, we developed a new protein pairwise similarity method (ProS) to compare and visualize the structural data generated in an MD run and to cluster the GPCR substructures sampled. To that end, we developed a GPCR-likeness assessment score (GLAS) that allows us to score the clusters according to their agreement with the GPCR conserved 24 inter-TM contacts as described by Venkatakrishnan et al.[61]

Finally, we validated our modeling results by extending the existing SDM data. Our particular interest was focused on position 4.60, located in the proximity of position 3.33 that was previously identified as being critical for antagonist binding and selectivity. Position 4.60 in TM4 is occupied by conserved residue Q179$^{4.60}$ in OX1 and Q187$^{4.60}$ in OX2.

## MATERIALS AND METHODS

**Residue Numbering.** We used both sequence number and the Ballesteros and Weinstein[39] numbering system to identify amino acid positions as described by us previously.[62] In the latter, transmembrane (TM) residues are given two numbers; the first is the TM helix number (1−7), while the second indicates the position relative to the most conserved residue in that TM, which is arbitrarily assigned to be 50. We number the loops in a similar manner; for example, the conserved cysteine in extracellular loop 2 (ECL2) would be labeled 45.50, to indicate its presence between TM4 and TM5.

**Multiple-Sequence Alignment, Homology Modeling, and Molecular Dynamics.** The production of a multiple-sequence alignment and template selection for homology modeling were conducted as previously described by us,[62] so here we give a brief account. Sequences of human OX1 (O43613) and human OX2 (O43614) were retrieved from Swiss-Prot database and aligned with four published crystal structures of GPCR receptors [bovine rhodopsin (PDB entry 1U19),[63] human dopamine D3 receptor (D3, PDB entry 3PBL),[64] human $A_{2A}$ adenosine receptor ($A_{2A}$, PDB entry 3EML),[65] and the $\beta$2-adrenergic receptor ($\beta$2AR, PDB entry 2RH1)],[66] using MOE (version 2010.10, Chemical Computing Group). Potential templates were ranked on the basis of the maximal number of correctly aligned prolines in the 7TMD. The D3 structure had the largest number of aligned prolines and was chosen as the template for homology modeling again using MOE, with the resulting model minimized using the MMFF94x force field.[67] To minimize the modeling "noise" between OX receptors and to generate equal starting points for further study, we used the hOX1 model as the template to model hOX2. The models were embedded in a 1-palmitoyl-2-oleoyl-*sn*-glycero-3-phosphocholine (POPC) bilayer using the *g_membed* feature of GROMACS[68] and an energy minimization with a steepest descent algorithm until convergence with a force tolerance of 0.239 kcal mol$^{-1}$ Å$^{-1}$ was performed. Sodium and chloride ions were then added to the systems to a concentration of 150 mM followed by a restrained MD run whereby all heavy atoms were restrained by a harmonic potential of 2.39 kcal mol$^{-1}$ Å$^{-2}$ for 200 ps. Finally, 50 ns production runs were performed on three repeats that differed in their initial velocities only. MD simulations were conducted with GROMACS version 4.5.4[69] using the OPLS-AA[70,71] force field and TIP3P water molecules[72] Production simulations were performed in an *NPT* ensemble maintained at 310 K and 1 bar. The integration time step was set to 2 fs, and a stochastic dynamics integrator[73] was used. Long-range electrostatics were calculated using the particle mesh Ewald (PME) method[74] with a 14 Å cutoff and 1 Å space grid. The Lennard-Jones potential used a cutoff of 9 Å, with a switch at 8 Å. The LINCS algorithm[75] was used to constrain bond lengths in both the lipid molecules and the protein.

**Ensemble-Flexible Docking Protocol.** We used the "ensemble-flexible docking protocol", a built-in function of the GOLD docking package (version 5.0, Cambridge Crystallographic Data Centre). The ensemble docking is a procedure that allows simultaneous docking of ligands into multiple substates (structures) of the same GPCR.[40,76] When multiple GPCR substates are available, one does not know *a priori* which substate will give the best docking performance. One strong advantage of ensemble docking is that it very significantly reduces the risk of inadvertently choosing an unsuitable substate model. In our case, the substates of Orexin receptors were retrieved from MD (see Figure 3) simulation runs.


**Figure 3.** Plot of the GPCR score vs the X-ray resolution of the 117 GPCR crystal structures extracted from the PDB. The color coding for each of the data points is based on its GPCR subfamily.

Ensemble docking in GOLD version 5.0 uses a genetic algorithm that makes this process more efficient with respect to sequential docking, which requires substantial postprocessing to identify the best ranking poses from the different docking experiments.[76]

We assigned flexibility to key residues in both receptors and peptides using the GOLD rotamer library to improve their steric fit and to ensure that the docking procedure could adjust the site to accommodate large molecules such as Orexin peptides. The list of key residues was taken from SDM data. In the case of OX1, the flexibility was assigned to nine residues: Q126$^{3.32}$, V130$^{3.36}$, D203$^{45.51}$, W206$^{45.54}$, Y215A$^{5.38}$, F219$^{5.42}$, Y224$^{5.47}$, Y311$^{6.48}$, and H344$^{7.39}$. In OX2, the flexibility was assigned to nine residues: Q134A$^{3.32}$, D211$^{45.51}$, W214$^{5.54}$, Y223$^{5.38}$, F227$^{5.42}$, Y232A$^{5.47}$, Y317A$^{6.48}$, F346$^{7.35}$, and H350$^{7.39}$. In the truncated C-terminus of OxA, the flexibility was assigned to nine residues: L16, L19, L20, N25, H26, I30, L31, T32, and L33. In the truncated C-terminus of OxB, the flexibility was assigned to nine residues: L11, L14, L15, N20, H21, I25, L26, T27, and M28.

We docked each conformer of the peptide independently into an ensemble of six receptor substates taken from MD. The docking poses were scored by the GOLD ChemPLP scoring function recommended for ensemble docking,[76,77] and we retained the 10 top-ranked docking poses for each receptor−peptide complex. The best pose of the receptor−peptide complex was selected on the basis of the maximal number of interactions between SDM-validated key residues of the

receptor and the peptide responsible for peptide potency and efficacy.

**Protein Pairwise Similarity (ProS).** We developed a new method, which we call ProS, to analyze and visualize the structural data generated via MD and to cluster the variety of GPCR substructures sampled by MD simulation. We used this tool to compare substates of OX receptors produced in our MD run. In this method, two proteins are considered similar if two conditions occurred simultaneously: (1) if the residues of the relevant pair have the same type evaluated by the substitution matrix *blosum65* and (2) if the "positions" and "directions" of the relevant residue pair are similar. In the case of GPCRs, the relevant residue pairs are considered for those residues that have the same Ballesteros and Weinstein index. The position and direction of each residue are defined by the coordinates of its C$\alpha$ and C$\beta$ atoms, respectively. We assume that if the distance between the C$\beta$ atoms of two relevant residues is small then the side chains of these residues can also adopt similar conformations. The global protein similarity score, $S^{\text{Protein-Similarity}}$, is calculated via eq 1:

$$S^{\text{Protein-Similarity}} = \frac{\text{SA}^{\text{scaled}}_{(\text{protein 1,protein 2})} + \text{SB}^{\text{scaled}}_{(\text{protein 1,protein 2})}}{2} \quad (1)$$

where $\text{SA}^{\text{scaled}}_{(\text{protein 1,protein 2})}$ describes the average similarity in positions and the term $\text{SB}^{\text{scaled}}_{(\text{protein 1,protein 2})}$ describes the average similarity in residue type and direction of the relevant residue pairs. The term $\text{SA}^{\text{scaled}}_{(\text{protein 1,protein 2})}$ is calculated via eq 2:

$$\text{SA}^{\text{scaled}}_{(\text{protein 1,protein 2})} = \frac{\sum_{i=1}^{N} \text{SA}^{i}_{(\text{protein 1,protein 2})}}{N} \quad (2)$$

where the score ranges between 0 and 1 (1 indicates 100% similar, and 0 means there is no similarity). $N$ is the number of the relevant pairs, and $\text{SA}^{i}_{(\text{protein 1,protein 2})}$ is the individual score calculated per pair using eq 3:

$$\text{SA}^{i}_{(\text{protein 1,protein 2})} = \text{e}^{-d_{C\alpha^i_1, C\alpha^i_2}} \quad (3)$$

where $d_{C\alpha^i_1, C\alpha^i_2}$ is the distance between C$\alpha$ atoms of the residues of relevant pair $i$ in proteins 1 and 2. The average $\text{SB}^{\text{scaled}}_{(\text{protein 1,protein 2})}$ is calculated in the same manner as $\text{SA}^{\text{scaled}}_{(\text{protein 1,protein 2})}$, and the similarity of residue type and direction of each relevant pair $\text{SB}^{i}_{(\text{protein 1,protein 2})}$ is calculated via eq 4:

$$\text{SB}^{i}_{(\text{protein 1,protein 2})} = \text{e}^{-\alpha d_{C\beta^i_1, C\beta^i_2}} \quad (4)$$

where $d_{C\beta^i_1, C\beta^i_2}$ is the distance between C$\beta$ atoms of the residues of relevant pair $i$ in proteins 1 and 2 and $\alpha$ is the substitution score taken from the blossum65 substitution matrix. ProS results are mapped back onto the proteins to allow visualization. Clustering based on ProS was performed using Ward's clustering method[78] as implemented in MOE.

**GPCR-Likeness Assessment Score (GLAS).** We also developed a GPCR-likeness assessment score (GLAS) to assess how "GPCR-like" our GPCR models and MD-derived structures (substates) are. GLAS is based on the conserved 24 inter-TM contacts as described by Venkatakrishnan et al.[61] In a comparison of the crystal structures of diverse GPCRs using a network representation, it was shown that some of the contacts between TM helices are conserved, in a manner independent of the sequence diversity or functional state of the given GPCR. A systematic analysis of the different GPCR structures, which includes both active and inactive states, revealed a consensus network of 24 inter-TM contacts mediated by 36 topologically equivalent amino acids. In this consensus network, the contacts are present in all (or all but one) of the structures, irrespective of their conformational state, and thus are likely to represent "molecular signatures" of the GPCR fold.[61] The significance of the residues in these positions is highlighted by the fact that mutations in 14 of 36 positions have been observed to result in either an increase or a loss of receptor activity.[79] The basic assumption in our GLAS scoring function is that high-quality GPCR models must show a large number of these 24 conserved contacts. Here we define that a pair of residues is in contact if the Euclidean distance between any pair of atoms (side chain and/or main chain atoms) is within the van der Waals interaction distance (that is, the sum of the van der Waals radii of the atoms plus 0.6 Å). The list of contacts obtained for the model is compared to the list of 24 conserved contacts. The overall GPCR score for the individual model is the number of its conserved contacts divided by 24 (the maximum), when the highest score is 1 (all 24 contacts are present) and the lowest score is 0 (none of the 24 contacts are present).

**Construction of Point-Mutated OX1 and OX2.** A combination of overlap and mismatch polymerase chain reaction (PCR) was used to introduce mutations into the corresponding Orexin-1 and Orexin-2 cDNAs as described by us previously.[62] Each mutation was made via the generation of two overlapping PCR fragments with PfuUltra II Fusion HS DNA Polymerase (Strategene). The two products were extracted, and a second round of PCR was performed via combination of both fragments with 5′ and 3′ gene specific primers (containing BamHI and NotI restriction sites, respectively). The resulting gel-purified products were then cloned into expression vector pFB-Neo for subsequent generation of stable cell lines. Constructs were confirmed via sequencing. Each verified cDNA was subsequently used to generate single, stably expressing clones in the CHO-K1 cell line.

**Calcium Flux Assays.** Standard calcium flux assays were used to assess the functionality of each OX receptor mutant. Each CHO-K1 Orexin mutant was seeded into tissue culture-treated, 384-well, black clear-bottom plates (CellBind Corning 7086), at a density of 7500 cells/well in culture medium and maintained in an incubator (5% $CO_2$ at 37 °C) overnight. The cell medium was removed, and the cells were incubated in 20 $\mu$L of assay buffer (4 $\mu$M Fluo-4AM in HBSS with 0.1% BSA) for 90 min at 37 °C. After incubation, the dye was removed and 45 $\mu$L of fresh buffer, without dye, was applied. Antagonists (5 $\mu$L) were applied, and after incubation for an additional 20 min at 37 °C, 20 $\mu$L of receptor specific agonists was applied and the calcium flux monitored using a Flex Station (Molecular Devices) over a period of 1 min. In all cases, the $EC_{80}$ specific for the individual mutant as determined in previous experiments was reported.

## RESULTS

**Evaluation of the GPCR Scoring Function (GLAS).** GLAS was calculated for 117 crystal structures of class A GPCRs stored in the PDB (see Table S1 of the Supporting Information). We plotted the GLAS for each crystal structure against its resolution (see Figure 3) and found that the average GLAS decreases with a decreasing resolution in a manner independent of GPCR subfamily; 12 high-resolution (≤2.5 Å)


dx.doi.org/10.1021/bi401119m | *Biochemistry* 2013, 52, 8246−8260

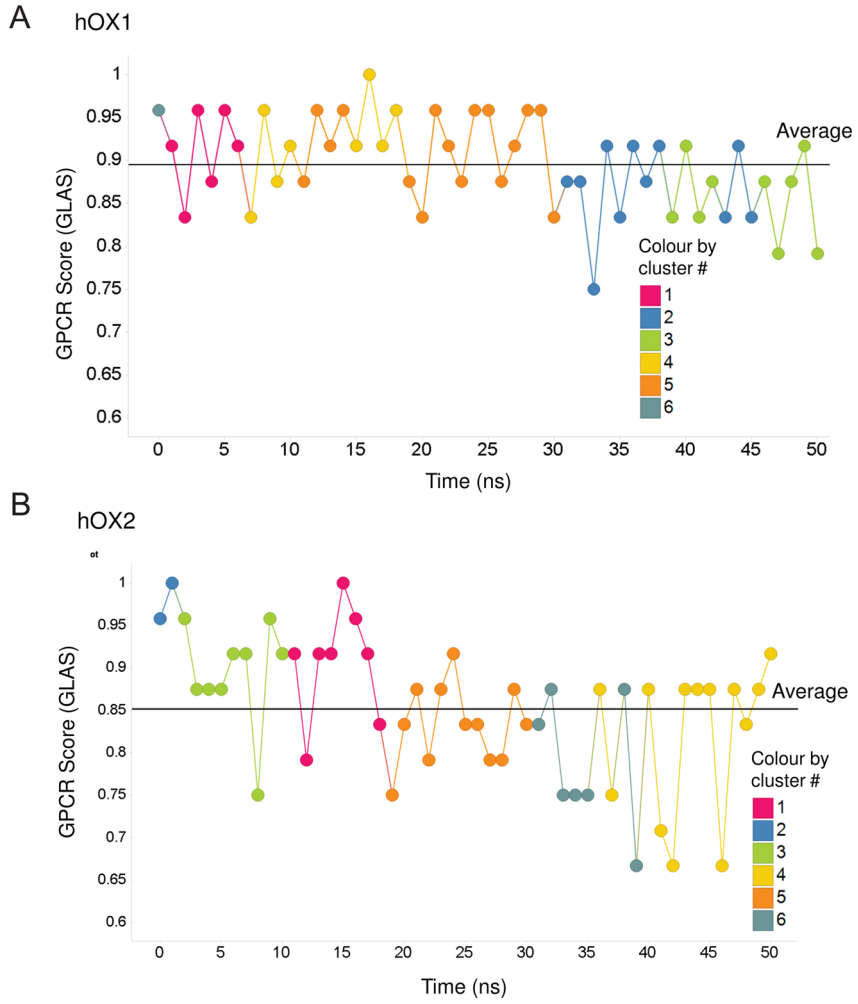


**Figure 4.** Plots of the GPCR score over time for a 50 ns MD simulation for hOX1 (A) and hOX2 (B) receptors, where the color coding is based on their cluster membership as defined by their ProS.

GPCR crystal structures have a GLAS on average of 0.99, 54 structures with a resolution in the range from 2.51 to 3.0 Å a GLAS on average of 0.98, 40 structures with a resolution in the range from 3.0 to 3.5 Å have a GLAS on average of 0.91, and 11 structures with a resolution of >3.5 Å have a GLAS on average of 0.91. The distribution of GLAS versus structure resolution is shown in Figure S1 of the Supporting Information. Although this result is intriguing, the data set is still quite small, and our main motivation for this procedure was to provide a means for assessing how "GPCR-like" our MD-derived structures are.

**Modeling of OX1 and OX2 Structures.** The modeling procedure of human OX1 and OX2 was as described by us previously.[62] Briefly, the homology model of the human OX1 receptor was modeled on the basis of a 2.8 Å high-resolution crystal structure of the dopamine D3 receptor (D3, PDB entry 3PBL). Of the possible templates available in the PDB at the time of preparation of this paper, D3 shared the greatest number of aligned prolines (five in total) with both hOX1 and hOX2 receptors, including the important proline in position 4.59.[66] The multiple-sequence alignment is shown in Figure S2 of the Supporting Information. Thus, D3 was preferred as the best template for OX receptor modeling. D3 has also a higher degree of sequence similarity with the hOX1 and hOX2 receptors than other GPCRs (65.5% when comparing just the 7TMD region). The homology model of hOX2 was constructed using the hOX1 model as a template. This was done to minimize the modeling noise between the OX receptors, to ease the comparison between them, and to generate equal starting points for the MD simulation studies. The homology models obtained for hOX1 and hOX2 receptors were employed as starting points for extensive MD simulations in an atomistic model of the membrane. It was observed that after 3 ns of MD, the C$\alpha$ atom fluctuations over time for all three MD simulation repeats were within the same narrow range of 1.7−2.4 Å,[62] which is comparable to the values typically obtained for MD simulations of GPCR crystal structures.[80]

**Clustering of OX1 and OX2 Structures.** Initially, we harvested 51 decoys (models) for each OX receptor from the MD run and homology modeling (one structure per nanosecond of the MD run over 50 ns plus one initial homology model). Then we calculated a protein similarity matrix (dimensions of 51 × 51) for these 51 decoys using the ProS method ($S^{\text{Protein-Similarity}}$; see the heat map describing this result in Figure S3A of the Supporting Information for OX1 and Figure S3B of the Supporting Information for OX2) as outlined in Materials and Methods. Next we used this ProS similarity matrix to cluster these 51 decoys using Ward's clustering method[78] (see the hierarchical agglomerative clustering tree in Figure S4 of the Supporting Information for OX1 and Figure


dx.doi.org/10.1021/bi401119m | *Biochemistry* 2013, 52, 8246−8260

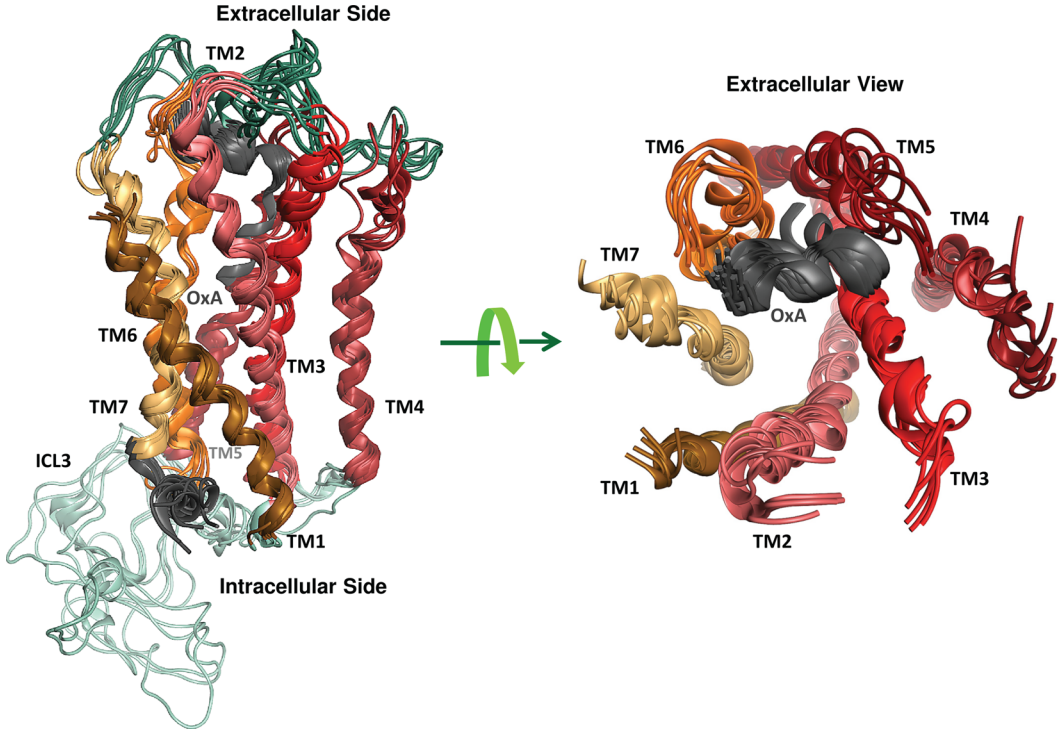


**Figure 5.** Six conformations of OX1 with the predicted docking poses of 30 conformations of the C-terminally truncated form of OxA (determined by NMR and extracted from PDB entry 1WSO).[34] Transmembrane domains 1−7 are colored dark orange, pink, red, purple, dark red, orange, and light yellow, respectively. Interstrand cross-links are colored cyan, ECLs dark green, and the C-termini of OxA and OX1 gray.

S5 of the Supporting Information for OX2) into six clusters. We also calculated the GLAS for each of these 51 decoys and plotted the change in GLAS versus time for the 50 ns MD simulation to evaluate how our simulated structures agree with known crystallographic structures in terms of key, well-conserved features among all GPCRs (see plots in Figure 4A for OX1 and Figure 4B for OX2). It can be seen that the MD structures are as good if not better in this regard than some of the lower-resolution X-ray structures, which we took as reassurance that the MD-generated structures are sensible. We took one representative conformer from each of the six clusters with the highest GLAS for further analysis and docking experiments. It is interesting that the GLAS tends to drift lower with time. However, it is still comparable to the range of GLAS values calculated for crystal structures. Regardless, in this work, we took the top-scored/ranked representative from each cluster observed that was >0.85 (see plots in Figure 4A for OX1 and Figure 4B for OX2), and therefore, we have no reason to suspect our level of confidence should be lower.

**Modeling the C-Terminus of OxA and OxB.** OxA coordinates were taken from the NMR-determined structure (PDB entry 1WSO[34]). We selected the NMR structure of OxA and not the X-ray structure because we were interested in exploring the conformational space of the peptide and not just one snapshot. This was required for our docking procedure. The low-energy "bioactive" conformation of the molecules can frequently be found among the conformations of this molecule in water.[81] The structure of the C-terminus of OxA in water[34] consists of two $\alpha$-helices (see Figure 2A) making various angles within a 60−80° range relative to each other and the flexible linker connecting these helices (Figure 2B). The 30 conformations of the C-terminus of OxB were homology modeled on the basis of the 30 conformations of OxA using the alignment as shown in Figure 2A with MOE (version 2010.10, Chemical Computing Group).

**Predicted Mode of Binding of OxA in OX1 and OX2.** The 30 conformations of OxA obtained from the NMR ensemble (PDB entry 1WSO) were docked into six conformers of OX1 harvested from MD using the ensemble-flexible docking protocol (see Figure 5). This protocol allows efficient docking of the peptide to the receptor as it is provides sufficient flexibility for both the receptor and the peptide. The 10 top-ranked complexes for OxA, based on the GOLD default scoring function,[77] were visually inspected. Of these 10 docking poses, the best pose of OxA in OX1 was selected on the basis of the maximal number of interactions between SDM-validated key residues of OX2 and OxA responsible for OxA potency and efficacy. The proposed docking pose of OxA in the OX1 binding site is shown in Figure 6A, and the two-dimensional (2D) interaction map is shown in Figure 6C. The OX1 binding site for OxA is formed by TMs 3 and 5−7. We explored if the key residues found in the SDM of OX1 generate interactions with the key residues found in the alanine scan of OxA. We predict that residue L16 forms van der Waals type interactions with H344$^{7.39}$, and D203$^{45.51}$ is in the proximity of L19 and could potentially form a nonclassical hydrogen bond.[82,83] Residues H344$^{7.39}$ and W206$^{45.54}$ generate a hydrophobic "sandwich" with L20 of OxA. Q126$^{3.34}$ forms an interaction with A27 of OxA. N25 is in the proximity of Y215$^{5.38}$ and could potentially make a hydrogen bond during the activation process. F219$^{5.42}$ forms a face-to-edge $\pi-\pi$ stack with H26. Residues Y224$^{5.47}$ and V130$^{3.36}$ generate another hydrophobic sandwich with I30. The Y311$^{6.48}$ side chain forms van der Waals interactions with L31, and the backbone of Y311$^{6.48}$ interacts with T32 of OxA (Figure 6A). These last two interactions seem to be essential for both the potency and the efficacy of OxA


dx.doi.org/10.1021/bi401119m | *Biochemistry* 2013, 52, 8246−8260

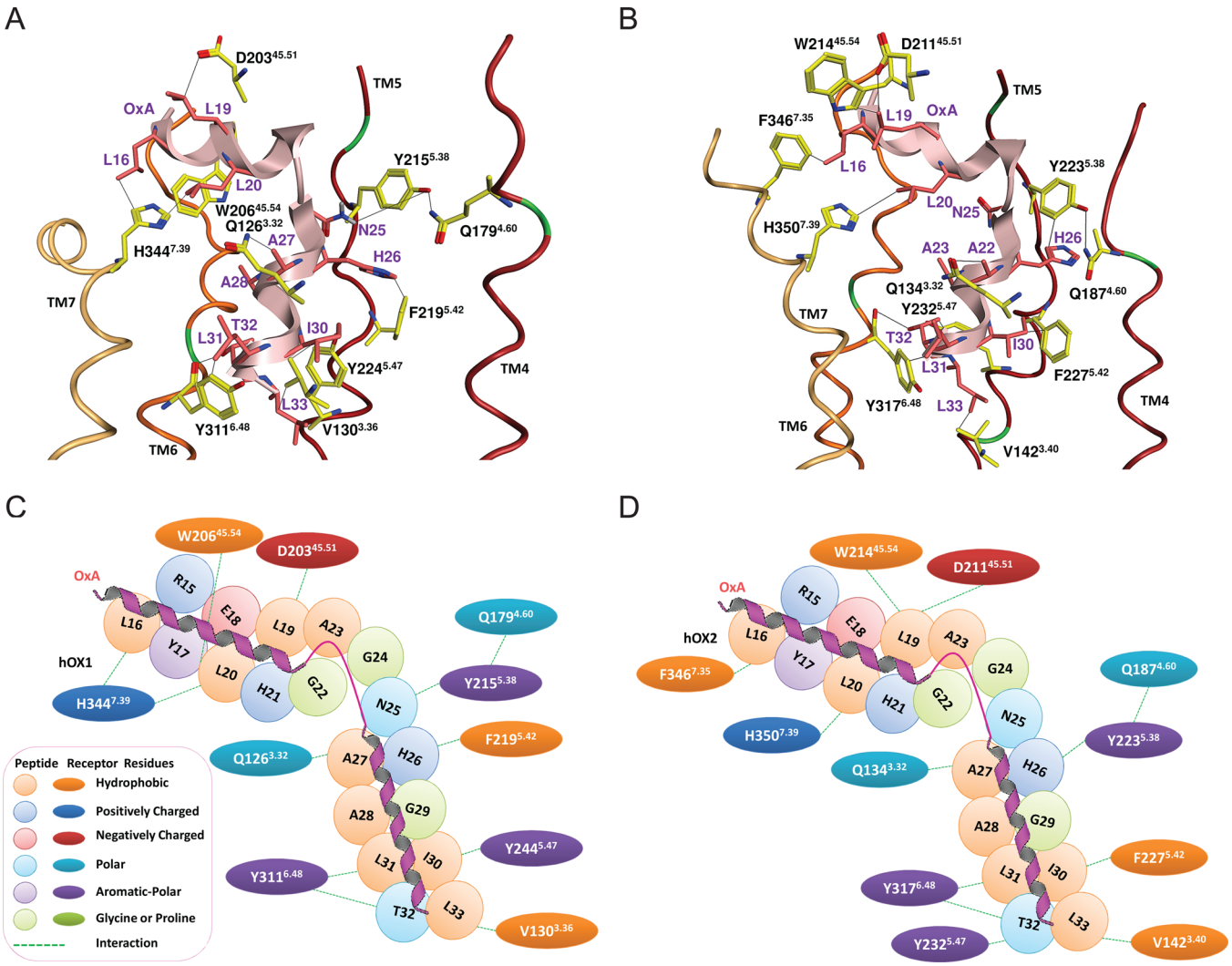


**Figure 6.** Best pose of OxA in OX1 (A and C) and OX2 (B and D) models. The loops, TM2 and TM3, were hidden to expose the binding pocket. Transmembrane domains 1−7 are colored dark orange, pink, red, purple, dark red, orange, and light yellow, respectively, and OxA is colored light pink. Only the key residues taken from SDM data are shown; carbon atoms of OxA are colored pink and those of receptors yellow. Nitrogen atoms are colored blue, oxygen atoms red, sulfur atoms yellow, and chlorine atoms light green. Interactions with key residues are indicated by black lines. Panels C and D show a two-dimensional interaction map between OxA and OX receptors.

agonism. The Y311A$^{6.48}$ mutation results in a large decrease in both the potency and the efficacy of OxA[37] and correlates with the same effect of the L31A mutation.[38] These predictions are supported by the fact that Y311$^{6.48}$ is part of the transmission switch (previously called the "toggle switch") that is proposed to play a role in GPCR activation.[84] Finally, L33 generates hydrophobic interactions with V130$^{3.36}$, which forms part of the conserved VSVSVAVL motif of TM3$^{OX1}$.

The same protocol was used to dock the same 30 conformations of OxA into OX2 (see panels B and D of Figure 6) and the same procedure used to evaluate the best pose. The predicted pose suggests that residue L16 forms a hydrophobic interaction with F346$^{7.35}$. D211$^{45.51}$ is in the proximity of L19. L19 and L20 form hydrophobic interactions with W214$^{45.54}$ and H350$^{7.39}$, respectively. Unlike OX1, N25 of OxA does not form a hydrogen bond with the tyrosine at position 5.38 (Y215$^{5.38}$ in OX1, but Y223$^{5.38}$ in OX2). In the case of OX2, Y223$^{5.38}$ forms an interaction with H26 of OxA. F227$^{5.42}$ forms a nonpolar interaction with I30. Y317$^{6.48}$ is in nonpolar contact with L31, and this interaction is essential for both the potency and the efficacy of OxA agonism. Mutating Y317$^{6.48}$ to alanine results in a decrease in potency of 17.7-fold and efficacy (relative $E_{max}$ decreases to 49.6%) of OxA,[37] which correlates with the L30A mutation in OxA that resulted in the abolishment of both the potency and the efficacy of OxA.[38] Similar to OX1, the peptide L33 residue interacts with V142$^{3.40}$. The side chain of T32 forms a hydrogen bond with the backbone of Y317$^{6.48}$ and a hydrophobic contact with Y232$^{5.47}$.

**Predicted Mode of Binding of OxB in OX1 and OX2.** The same procedure was performed for binding of OxB to OX1 and OX2. The predicted docking pose of OxB in OX1 is shown in Figure 7A along with a 2D interaction map in Figure 7C. The OX1−OxB binding site is formed by TM3 and TM5−7. Unsurprisingly, but reassuringly, we find similar interaction patterns for the OxB peptide compared to the OxA peptide. We predict that L11 of OxB forms a nonpolar interaction with H344$^{7.39}$. This same histidine along with W206$^{45.54}$ generates a hydrophobic sandwich with L15. D203$^{45.51}$ is in the proximity of L14 and could potentially form a nonclassical hydrogen bond.[82,83] A potential salt bridge can be formed between R15 and D203$^{45.51}$. Y215$^{5.38}$ and N20 are in the proximity of each other and with a slight adjustment could potentially form a


dx.doi.org/10.1021/bi401119m | *Biochemistry* 2013, 52, 8246−8260

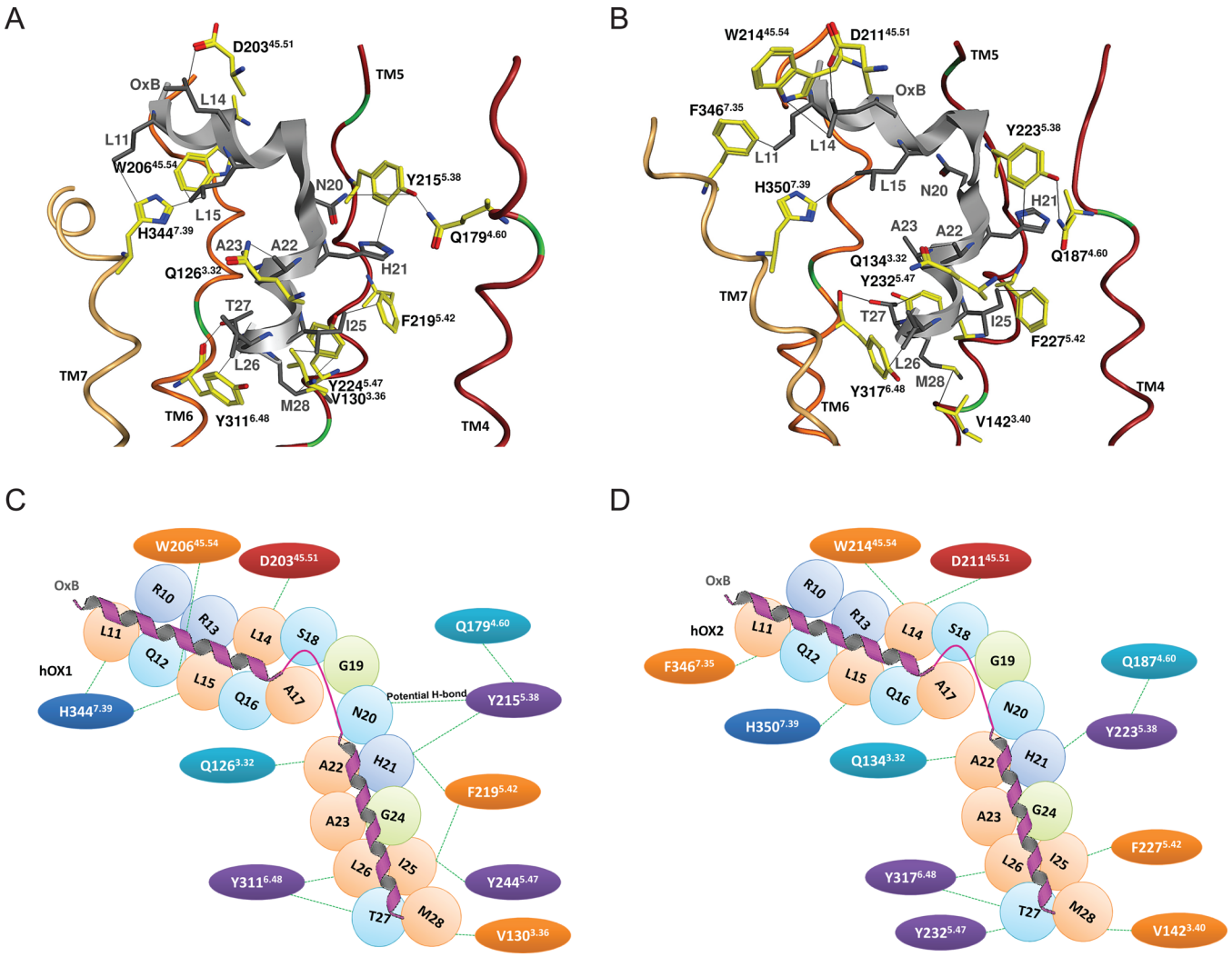


**Figure 7.** Best pose of OxB in OX1 (A and C) and OX2 (B and D) models. The loops, TM2 and TM3, were hidden to expose the binding pocket. Transmembrane domains 1−7 are colored dark orange, pink, red, purple, dark red, orange, and light yellow, respectively, and OxB is colored gray. Only the key residues taken from SDM data are shown; carbon atoms of OxB are colored gray and those of receptors yellow. Nitrogen atoms are colored blue, oxygen atoms red, sulfur atoms yellow, and chlorine atoms light green. Interactions with key residues are indicated by black lines. Panels C and D show a two-dimensional interaction map between OxB and OX receptors.

reasonable hydrogen bond. Residue F219$^{5.42}$ forms a nonpolar interaction with H21. Residues Y224$^{5.47}$ and V130$^{3.36}$ generate a nonpolar sandwich with I25. Y311$^{6.48}$ interacts with L26, and the side chain of T27 forms a hydrogen bond with the backbone of Y311$^{6.48}$. Similar to the situation for OxA, these last two interactions seem to be essential for both the potency and the efficacy of OxB agonism. The Y311A$^{6.48}$ mutation resulted in a large decrease in both the potency and the efficacy of OxB[37] and correlates with the same effect of the L26A mutation, which results in the abolishment of both the potency and the efficacy of OxB.[36] Finally, M28 forms a hydrophobic interaction with Y224$^{5.47}$.

The OX2−OxB binding pose (Figure 7B,D) predicts that residue L11 forms a nonpolar interaction with F346$^{7.35}$, L14 interacts with W214$^{45.54}$, and H350$^{7.39}$ forms a hydrophobic interaction with L15 of OxB. As was the case for OX2−OxB interactions, D211$^{45.51}$ is in the proximity of L14 and could potentially form a nonclassical hydrogen bond,[82,83] and a potential salt bridge could be formed between R15 and D203$^{45.51}$. Unlike the case in OX1, Y223$^{5.38}$ (the equivalent in OX1 is Y215$^{5.38}$) does not interact with N20. F227$^{5.42}$ forms a nonpolar interaction with I25, and Y317$^{6.48}$ generates hydrophobic complementarity with L26. Substituting L26 with a D-amino acid resulted in 17000-fold decrease in $EC_{50}$ compared to that of the wild type.[36] As stated before, this latter interaction is likely to be centrally important. M28 forms nonpolar interactions with V142$^{3.40}$. The side chain of T32 generates a hydrogen bond with the backbone of Y317$^{6.48}$. On the basis of the SDM data and these modeling observations, it seems that helix 2 of OxA and OxB is playing a major role in Orexin receptor binding and activation.

## DISCUSSION

SDM data that have been produced independently for Orexin receptors and for peptides were paired by homology modeling, MD simulation, and ensemble-flexible docking to isolate the key interactions responsible for agonist potency and efficacy. This working model should be useful for the design of nonpeptidic Orexin agonists together with improving the chances of designing selective or "biased" antagonists. In this work, we demonstrate the usefulness of a new, protein pairwise similarity method (ProS) and a GPCR scoring function


dx.doi.org/10.1021/bi401119m | Biochemistry 2013, 52, 8246−8260

(GLAS) in analyzing structural data produced by MD simulations. We used homology modeling followed by MD simulation and flexible docking to generate docking poses of Orexins in the inactive or semiactive forms of the OX receptors. We flexibly docked the Orexin peptides into post-MD substates of inactive forms of Orexin receptors.

The docked modes along with the SDM data suggest that helix 2 of OxA and OxB (see Figure 2A) plays a major role in Orexin receptor binding and activation. Mutation of any helix 2 residue (A29−L33 in OxA and A24−M28 in OxB) to alanine (or in case of alanine to glycine) resulted in an almost total loss of the peptides' potency and efficacy for both Orexin receptors (see Table 2). It seems that for A28 in OxA and A23 in OxB, mutation to glycine has an impact on the $\alpha$-helical conformation of the peptides. Glycine residues tend to disrupt helices because of their high conformational flexibility, which consequently makes it entropically expensive to adopt the relatively constrained $\alpha$-helical structure needed to bind to the receptor.[85] The $\alpha$-helical nature of the Orexin peptides in this area is apparently essential for a bioactive conformation and consequent potency and efficacy.

It seems that the aromatic nature of $Y^{6.48}$ in both receptors is critical for the potency of both agonists. Mutation of $Y^{6.48}$ to alanine significantly reduces agonist potency[37] (see Table 1) for both receptors, but mutation of $Y^{6.48}$ to phenylalanine had almost no effect on potency. According to our model, $Y^{6.48}$ in both receptors generates a hydrophobic overlay with the conserved residues, L31 in OxA and L26 in OxB. This interaction seems to be very important for both the potency and the activation by both agonists because (i) the $Y^{6.48}A$ mutation in the receptors, L31A in OxA or L26A in OxB, kills both potency and efficacy and (ii) $Y^{6.48}$ is part of the transmission switch (previously called the toggle switch) that is associated with GPCR activation.[84] Furthermore, the predicted binding modes suggest that the backbone carbonyl of $Y^{6.48}$ forms an interaction with T32 (in OxA) and T27 (in OxB). Mutation of T32 or T27 in OxA or OxB, respectively, results in a loss of potency.

Mutation of $Y^{5.47}$ to alanine resulted in a significant decrease in OxA potency. $Y^{5.47}$ interacts with T32 when OxA is bound to OX1 and with I30 when OxA is bound to OX2. Because residues T32 and I30 are both essential for the potency of OxA, we predict that interactions between $Y^{5.47}$ and T32 and I30 are critical for receptor activation by OxA. We note that position 5.47 has been found to be involved in agonist binding in other receptors; for example, it plays a role in the binding and activation of $\beta$2-adrenergic receptor agonists.[86]

C-Terminal residues, L33 in OxA and M28 in OxB, appear to play an important role in the activation process. Mutation of these residues to alanine almost abolished potency. We observed that these residues form shape complementarity with the subpocket generated by the VSVSVAVL motif of $TM3^{OX1}$ or VSVSVSVL motif of $TM3^{OX2}$. Our results suggest that these long terminal residues, L33 in OxA and M28 in OxB, are responsible for "anchoring" the agonists in the receptor pockets. The OX1 subpocket is more hydrophobic than the OX2 subpocket, because of the presence of alanine at position X in the VSVSVXVL motif in $TM3^{OX1}$ compared to a serine in $TM3^{OX2}$. This small difference can impact the subtype selectivity of the peptides. For OxA, L33 generates a nonpolar interaction with $V130^{3.36}$ that is part of the conserved VSVSVAVL motif of $TM3^{OX1}$ (see Figure 6A). The $V130A^{3.36}$ mutation in OX1 reduces the potency by 30.6-fold. However, the $V138A^{3.36}$ mutation of $TM3^{OX2}$ had no impact on potency (see Table 1). In our model, L33 of OxA interacts with another valine ($V142^{3.40}$) that is also part of the conserved VSVSVSVL motif of $TM3^{OX2}$ (see Figure 6B). The same types of interactions are also formed between M28 of OxB and $V130^{3.36}$ in OX1 (see Figure 7A) and between M28 of OxB and $V142^{3.40}$ in OX2[36] (see Figure 7B). The involvement of TM3 in most GPCR activation processes is a very common phenomenon that has been extensively described in the literature.[61,87]

We also explored the role of the conserved $F^{5.42}$. The mutation of this residue to alanine in both receptors reduces the potencies for OxA (see Table 1) and efficacy of OxA in OX2 to 64.3%.[37] However, the decrease in potency in the case of OX2 was doubled (240.3-fold) compared to that of OX1 (139.6-fold) (see Table 1). In the case of OX1, $F^{5.42}$ interacts with H26 of OxA that, based on the SDM experiments, has an only moderate impact on potency (see Figure 6A). This is in contrast to OX2 in which $F^{5.42}$ interacts with key residue I30 (see Figure 6B). Mutation of I30 of OxA to alanine completely abolished the potency of OxA for both receptors [in the case of OX1, I30 interacts with $Y224^{5.47}$ (see Figure 6A)]. It seems that in the case of OxB, $F^{5.42}$ plays a key role in potency for both receptors, by interacting with key residue I25 (see Figure 7A,B). This observation is supported by the SDM data: mutation of $F^{5.42}$ to tryptophan abolishes the potency of OxB with respect to OX2 (see Table 1), and mutation of I25 to alanine abolishes the potency of OxB for both receptors (see Table 2).

The role of the conserved $Y^{5.38}$ was also clarified when mutation of this residue to alanine resulted in the abolishment of OxA potency (see Table 1) and a moderate loss of efficacy[37] for both receptors. According to the model, $Y^{5.38}$ is located near the linker (kink) connecting helix 1 and helix 2 of the peptides (see Figure 6A for OX1 and Figure 6B for OX2). We hypothesize that $Y^{5.38}$ can play a role in stabilizing the relative angle between helix 1 and helix 2 and, by doing so, helps to stabilize the bioactive conformation of OxA in the same mode as OxB (see Figure 7). In the case of OX1, this effect can be supported by the observation that $Y215^{5.38}$ can potentially form a hydrogen bond with N25 of OxA that is located at the beginning of this flexible linker. However, the generation of this hydrogen bond is hindered by the interhelical hydrogen bond between $Y215^{5.38}$ and $Q179^{4.60}$ that limits $Y215^{5.38}$ flexibility. To validate this hypothesis, we mutated $Q179^{4.60}$ to alanine, predicting that by breaking this interhelical hydrogen bond we will "release" the $Y215^{5.38}$ to generate a hydrogen bond with N25, and indeed, it resulted in a 17.8-fold improvement in the potency of OxA with respect to OX1 (see Table 1). In the case of OX2, however, the model predicts that N25 would not form a hydrogen bond with $Y215^{5.38}$. As predicted when we mutated $Q187^{4.60}$ (that forms a hydrogen bond with $Y215^{5.38}$) to alanine, we observed no effect on the binding of OxA to OX2 (see Table 1). Although these results concerning potency agree well with the prediction, we should caution the reader that the experiments are based on our $Ca^{2+}$ concentration assay and thus do not preclude other possibilities such as destabilization of native states or inhibition of the transition from inactive to active in other ways.

Analogous to the potential interaction between N25 of OxA and $Y215^{5.38}$, N20 of OxB can potentially form a similar interaction, which again would be hindered by the presence of the interhelical hydrogen bond between $Y215^{5.38}$ and $Q179^{4.60}$.

We predicted that, in a fashion similar to that of OxA, OxB would be able to form a hydrogen bond via N20 to Y215$^{5.38}$ if Q179$^{4.60}$ were mutated to alanine. Consistent with this prediction, the potency of OxB at OX1 was observed to increase 72.2-fold (Table 1). In OX2, we predicted that N20 of OxB does not form a hydrogen bond to Y215$^{5.38}$; thus, mutating Q187$^{4.60}$ in this case would not be expected to affect OxB binding, which, again, we observed (Table 1).

An additional residue that plays a key role in OX receptor agonist binding and activation by Orexin peptides is H$^{7.39}$. Mutation of this residue to alanine resulted in a severe decrease in the potency of OxA (see Table 1) and in 64.5 and 63.0% decreases in its $E_{max}$ values for OX1 and OX2, respectively.[37] We observed that in OX1, H$^{7.39}$ interacts with residues L16 and L20 of helix 1 of OxA (see Figure 6A). Mutation of L16 or L20 of OxA to alanine resulted in a loss of potency of OxA with respect to OX1. On the other hand, in OX2, H$^{7.39}$ interacts with L20 and not with L16 (see Figure 6B), and this observation is supported by the SDM data; mutation of L16 to alanine had no effect on the binding of OxA to OX2 compared to the dramatic effect of mutating L20. In the case of OxB, we do not have SDM data for H$^{7.39}$; however, we predict that H$^{7.39}$ interacts with residues L11 and L15 of helix 1 of OxB (see Figure 7A). Mutation of L11 or L15 of OxB to alanine resulted in a loss of potency of OxB with respect to OX1. On the other hand, in OX2, H$^{7.39}$ interacts with L15 only, and not with L11 (see Figure 7B). This observation is supported by the SDM data; mutation of L11 to alanine had no effect on the binding of OxB to OX2 compared to a dramatic effect observed for mutating L15, where a similar selective effect was previously observed by Asahi et al.[36]

Mutation of D$^{45.51}$ and W$^{45.54}$ can also be beneficial for agonist potency. The mutation of these residues to alanine resulted in a loss of potency of OxA for both receptors. We predict that D$^{45.51}$ generates a steric effect with L19 of OxA for both receptors and W$^{45.54}$ interacts with L20 of OxA when binding to OX1 (see Figure 6A) and with L19 in OxA when binding to OX2 (see Figure 6B).

It seems to be primarily residues of TM3, -5, and -6 that are involved in both the potency and the efficacy of the agonists. For the discovery of novel nonpeptidic Orexin agonists, we recommend, on the basis of these results, that the main targets for ligand design should be interactions with Y$^{6.48}$, the hydrophobic motif of VSVSV<u>X</u>VL in TM3, Y$^{5.38}$, F$^{5.42}$, Y$^{5.47}$, and H$^{7.39}$. Interaction with D$^{45.51}$ and W$^{45.54}$ can be beneficial for binding of both agonists and antagonists, as shown in our previous publication.[62]

In terms of how the result might be interpreted with respect to activation, it seems that the binding of large molecules, like OxA and OxB peptides, to the interior space of the receptor destabilizes its most populated inactive state and, by doing so, promotes the receptor toward the active state. OxA and OxB peptides disturb noncovalent interactions between different TMs, especially the link between TM3 and TM6 formed in the binding site by S$^{3.35}$ and Y$^{6.48}$ and the hydrophobic triad of V$^{3.40}$, L$^{3.43}$, and F$^{6.44}$. We observed that hydrogen bonds between S$^{3.35}$ and Y$^{6.48}$ (defined when the distance between oxygen atoms of the OH group of S$^{3.35}$ and Y$^{6.48}$ is ≤3.5 Å) appear at a frequency of >90% for MD runs of inactive OX1 and >85% for inactive OX2. We observed that the hydrophobic triad of V$^{3.40}$, L$^{3.43}$, and F$^{6.44}$ (defined as present when the distance between the side chain carbon atoms of V$^{3.40}$, L$^{3.43}$, and F$^{6.44}$ is ≤4.5 Å) appears at a frequency of >90% for MD runs of OX1 and OX2. The loss of these interactions potentially has a negative effect on the stability of the inactive state of OX receptors and may induce activation due to the fact that F$^{6.44}$ and Y$^{6.48}$ are also part of the transmission switch. The transmission switch includes a relocation of conserved residues, such as F$^{6.44}$ and Y$^{6.48}$, toward P$^{5.50}$. This newly discovered[84] and larger switch links the agonist binding site with the movement of TM5 and TM6 through rearrangement of the TM3−TM5−TM6 interface.

## CONCLUSION

The MD simulation protocol used in our work, followed by ensemble-flexible docking, has gone beyond the use of static models and allowed for a more detailed exploration of the OX structures. In this work, we have demonstrated how these methods in combination with SDM data and newly developed post-MD analysis tools can deal with the flexibility of GPCRs to rationalize not only binding affinity but also the potency, efficacy and selectivity of GPCR agonists. The MD simulations allow the prediction of GPCR substates that is not possible with static homology modeling alone.

## ASSOCIATED CONTENT

### Supporting Information

Details of the structures used for the development of the ProS scoring function, the multiple-sequence alignment, and MD snapshot analysis. This material is available free of charge via the Internet at http://pubs.acs.org.

## AUTHOR INFORMATION

### Corresponding Authors

*E-mail: alexander.heifetz@evotec.com. Telephone: +44 1865 613305.

*E-mail: philip.biggin@bioch.ox.ac.uk.

### Funding

We are grateful to the Royal Society for an Industry Award granted to A.H. and to the BBSRC (G.B.M.).

### Notes

The authors declare no competing financial interest.

## ACKNOWLEDGMENTS

We are grateful to Dr. Markus Kosner and Dr. Simon Grimshaw from Chemical Computing Group for their help in developing the ProS method and the Ballesteros and Weinstein SVL script and Dr. Daniel Warner for his useful discussion about the development of GLAS.

## ABBREVIATIONS

OX, Orexin receptor; OX1, OX1R_HUMAN, Orexin-1 receptor; OX2, OX2R_HUMAN, Orexin-2 receptor; OxA, human Orexin-A peptide; OxB, human Orexin-B peptide; MD, molecular dynamics; SDM, site-directed mutagenesis; GPCRs, G-protein-coupled receptors; 3D, three-dimensional; 7TMD, seven-transmembrane domain; TM, transmembrane helix; ECL, extracellular loop; $\beta$2AR, $\beta$2-adrenergic receptor; PDB, Protein Data Bank; ProS, protein pairwise similarity score; GLAS, GPCR-likeness assessment score; WT, wild type; NMR, nuclear magnetic resonance.

## REFERENCES

(1) Azizi, H., Mirnajafi-Zadeh, J., Rohampour, K., and Semnanian, S. (2010) Antagonism of orexin type 1 receptors in the locus coeruleus

attenuates signs of naloxone-precipitated morphine withdrawal in rats. *Neurosci. Lett. 482*, 255−259.
(2) Cid-Pellitero, E. D., and Garzón, M. (2011) Hypocretin1/OrexinA-containing axons innervate locus coeruleus neurons that project to the Rat medial prefrontal cortex. Implication in the sleep-wakefulness cycle and cortical activation. *Synapse 65*, 843−857.
(3) Laburthe, M., Voisin, T., and El Firar, A. (2010) Orexins/hypocretins and orexin receptors in apoptosis: A mini-review. *Acta Physiol. 198*, 393−402.
(4) Mazza, M., Della, M. G., Paciello, N., Mennuni, G., Bria, P., and Mazza, S. (2005) Orexin, sleep and appetite regulation: A review. *Clin. Ter. 156*, 393−402.
(5) Acuna-Goycolea, C., and van den Pol, A. N. (2009) Neuroendocrine proopiomelanocortin neurons are excited by Hypocretin/Orexin. *J. Neurosci. 29*, 1503−1513.
(6) Toshinai, K., Yamaguchi, H., Kageyama, H., Matsuo, T., Koshinaka, K., Sasaki, K., Shioda, S., Minamino, N., and Nakazato, M. (2010) Neuroendocrine regulatory peptide-2 regulates feeding behavior via the orexin system in the hypothalamus. *Am. J. Physiol. 299*, E394−E401.
(7) Mieda, M., and Sakurai, T. (2013) Orexin (Hypocretin) receptor agonists and antagonists for treatment of sleep disorders. *CNS Drugs 27*, 83−90.
(8) Mieda, M., Tsujino, N., and Sakurai, T. (2013) Differential roles of orexin receptors in the regulation of sleep/wakefulness. *Front. Endocrinol. 4*, 57.
(9) Borgland, S. L., Taha, S. A., Sarti, F., Fields, H. L., and Bonci, A. (2006) Orexin A in the VTA is critical for the induction of synaptic plasticity and behavioral sensitization to cocaine. *Neuron 49*, 589−601.
(10) Choi, D. L., Davis, J. F., Fitzgerald, M. E., and Benoit, S. C. (2010) The role of orexin-A in food motivation, reward-based feeding behavior and food-induced neuronal activation in rats. *Neuroscience 167*, 11−20.
(11) Benoit, S. C., Clegg, D. J., Woods, S. C., and Seeley, R. J. (2005) The role of previous exposure in the appetitive and consummatory effects of orexigenic neuropeptides. *Peptides 26*, 751−757.
(12) Rodgers, R. J., Halford, J. C. G., Nunes de Souza, R. L., Canto de Souza, A. L., Piper, D. C., Arch, J. R. S., Upton, N., Porter, R. A., Johns, A., and Blundell, J. E. (2001) SB-334867, a selective orexin-1 receptor antagonist, enhances behavioural satiety and blocks the hyperphagic effect of orexin-A in rats. *Eur. J. Neurosci. 13*, 1444−1452.
(13) Sakurai, T. (2007) [Regulatory mechanism of sleep/wakefulness states by orexin]. *Tanpakushitsu Kakusan Koso 52*, 1840−1848.
(14) Li, Y., Li, S., Wei, C., Wang, H., Sui, N., and Kirouac, G. (2010) Orexins in the paraventricular nucleus of the thalamus mediate anxiety-like responses in rats. *Psychopharmacology 212*, 251−265.
(15) Scheurink, A. J. W., Boersma, G. J., Nergårdh, R., and Södersten, P. (2010) Neurobiology of hyperactivity and reward: Agreeable restlessness in Anorexia Nervosa. *Physiol. Behav. 100*, 490−495.
(16) Suzuki, M., Beuckmann, C. T., Shikata, K., Ogura, H., and Sawai, T. (2005) Orexin-A (hypocretin-1) is possibly involved in generation of anxiety-like behavior. *Brain Res. 1044*, 116−121.
(17) Cox, C. D., Breslin, M. J., Whitman, D. B., Schreier, J. D., McGaughey, G. B., Bogusky, M. J., Roecker, A. J., Mercer, S. P., Bednar, R. A., Lemaire, W., Bruno, J. G., Reiss, D. R., Harrell, C. M., Murphy, K. L., Garson, S. L., Doran, S. M., Prueksaritanont, T., Anderson, W. B., Tang, C., Roller, S., Cabalu, T. D., Cui, D., Hartman, G. D., Young, S. D., Koblan, K. S., Winrow, C. J., Renger, J. J., and Coleman, P. J. (2010) Discovery of the dual Orexin receptor antagonist [(7R)-4-(5-chloro-1,3-benzoxazol-2-yl)-7-methyl-1,4-diazepan-1-yl][5-methyl-2-(2H-1,2,3-triazol-2-yl)phenyl]methanone (MK-4305) for the treatment of insomnia. *J. Med. Chem. 53*, 5320−5332.
(18) Nollet, M., and Leman, S. (2013) Role of Orexin in the pathophysiology of depression: Potential for pharmacological intervention. *CNS Drugs 27*, 411−422.
(19) Nollet, M., Gaillard, P., Minier, F., Tanti, A., Belzung, C., and Leman, S. (2011) Activation of orexin neurons in dorsomedial/perifornical hypothalamus and antidepressant reversal in a rodent model of depression. *Neuropharmacology 61*, 336−346.
(20) Nollet, M., Gaillard, P., Tanti, A., Girault, V., Belzung, C., and Leman, S. (2012) Neurogenesis-independent antidepressant-like effects on behavior and stress axis response of a dual Orexin receptor antagonist in a rodent model of depression. *Neuropsychopharmacology 37*, 2210−2221.
(21) Katsuki, H., and Michinaga, S. (2012) Chapter fifteen: Anti-parkinson drugs and Orexin neurons. In *Vitamins & Hormones* (Gerald, L., Ed.) pp 279−290, Academic Press, New York.
(22) Mieda, M., and Sakurai, T. (2012) Overview of orexin/hypocretin system. *Prog. Brain Res. 198*, 5−14.
(23) Rajagopal, S., Rajagopal, K., and Lefkowitz, R. J. (2010) Teaching old receptors new tricks: Biasing seven-transmembrane receptors. *Nat. Rev. Drug Discovery 9*, 373−386.
(24) Dalrymple, M. B., Jaeger, W. C., Eidne, K. A., and Pfleger, K. D. G. (2011) Temporal profiling of Orexin receptor-arrestin-ubiquitin complexes reveals differences between receptor subtypes. *J. Biol. Chem. 286*, 16726−16733.
(25) Nijmeijer, S., Vischer, H. F., Rosethorne, E. M., Charlton, S. J., and Leurs, R. (2012) Analysis of multiple histamine H4 receptor compound classes uncovers G$\alpha$i protein- and $\beta$-Arrestin2-biased ligands. *Mol. Pharmacol. 82*, 1174−1182.
(26) Scammell, T. E., and Winrow, C. J. (2011) Orexin receptors: Pharmacology and therapeutic opportunities. *Annu. Rev. Pharmacol. Toxicol. 51*, 243−266.
(27) Yanagisawa, M. (2011) Hypothalamic orexin system: From orphan GPCR to therapeutic target. *Exp. Anim. 60*, 199.
(28) Fujimoto, T., Kunitomo, J., Tomata, Y., Nishiyama, K., Nakashima, M., Hirozane, M., Yoshikubo, S.-i., Hirai, K., and Marui, S. (2011) Discovery of potent, selective, orally active benzoxazepine-based Orexin-2 receptor antagonists. *Bioorg. Med. Chem. Lett. 21*, 6414−6416.
(29) Perrey, D. A., Gilmour, B. P., Runyon, S. P., Thomas, B. F., and Zhang, Y. (2011) Diaryl urea analogues of SB-334867 as orexin-1 receptor antagonists. *Bioorg. Med. Chem. Lett. 21*, 2980−2985.
(30) Lebold, T. P., Bonaventure, P., and Shireman, B. T. (2013) Selective orexin receptor antagonists. *Bioorg. Med. Chem. Lett. 23*, 4761−4769.
(31) Piper, D. C., Upton, N., Smith, M. I., and Hunter, A. J. (2000) The novel brain neuropeptide, orexin-A, modulates the sleep−wake cycle of rats. *Eur. J. Neurosci. 12*, 726−730.
(32) Lee, J.-H., Bang, E., Chae, K.-J., Kim, J.-Y., Lee, D. W., and Lee, W. (1999) Solution structure of a new hypothalamic neuropeptide, human hypocretin-2/orexin-B. *Eur. J. Biochem. 266*, 831−839.
(33) Sakurai, T., Amemiya, A., Ishii, M., Matsuzaki, I., Chemelli, R. M., Tanaka, H., Williams, S. C., Richardson, J. A., Kozlowski, G. P., Wilson, S., Arch, J. R. S., Buckingham, R. E., Haynes, A. C., Carr, S. A., Annan, R. S., McNulty, D. E., Liu, W.-S., Terrett, J. A., Elshourbagy, N. A., Bergsma, D. J., and Yanagisawa, M. (1998) Orexins and Orexin Receptors: A family of hypothalamic neuropeptides and G Protein-Coupled Receptors that regulate feeding behavior. *Cell 92*, 573−585.
(34) Takai, T., Takaya, T., Nakano, M., Akutsu, H., Nakagawa, A., Aimoto, S., Nagai, K., and Ikegami, T. (2006) Orexin-A is composed of a highly conserved C-terminal and a specific, hydrophilic N-terminal region, revealing the structural basis of specific recognition by the orexin-1 receptor. *J. Pept. Sci. 12*, 443−454.
(35) Ammoun, S., Lindholm, D., Wootz, H., Åkerman, K. E. O., and Kukkonen, J. P. (2006) G-protein-coupled OX1 Orexin/hcrtr-1 Hypocretin receptors induce caspase-dependent and -independent cell death through p38 mitogen-/stress-activated protein kinase. *J. Biol. Chem. 281*, 834−842.
(36) Asahi, S., Egashira, S.-I., Matsuda, M., Iwaasa, H., Kanatani, A., Ohkubo, M., Ihara, M., and Morishima, H. (2003) Development of an orexin-2 receptor selective agonist, [Ala11, d-Leu15]orexin-B. *Bioorg. Med. Chem. Lett. 13*, 111−113.
(37) Malherbe, P., Roche, O., Marcuz, A., Kratzeisen, C., Wettstein, J. G., and Bissantz, C. (2010) Mapping the Binding Pocket of Dual Antagonist Almorexant to Human Orexin 1 and Orexin 2 Receptors: Comparison with the Selective OX1 Antagonist SB-674042 and the Selective OX2 Antagonist N-Ethyl-2-[(6-methoxy-pyridin-3-yl)-(tol-

uene-2-sulfonyl)-amino]-N-pyridin-3-ylmethyl-acetamide (EMPA). *Mol. Pharmacol. 78*, 81−93.
(38) Darker, J. G., Porter, R. A., Eggleston, D. S., Smart, D., Brough, S. J., Sabido-David, C., and Jerman, J. C. (2001) Structure−activity analysis of truncated orexin-A analogues at the orexin-1 receptor. *Bioorg. Med. Chem. Lett. 11*, 737−740.
(39) Ballesteros, J. A., and Weinstein, H. (1995) Integrated methods for construction three dimensional models and computational probing of structure-function relations in G protein-coupled receptors. *Methods Neurosci. 25*, 366−428.
(40) Kim, T. H., Chung, K. Y., Manglik, A., Hansen, A. L., Dror, R. O., Mildorf, T. J., Shaw, D. E., Kobilka, B. K., and Prosser, R. S. (2013) The role of ligands on the equilibria between functional states of a G protein-coupled receptor. *J. Am. Chem. Soc. 135*, 9465−9474.
(41) Granier, S., Kim, S., Shafer, A. M., Ratnala, V. R. P., Fung, J. J., Zare, R. N., and Kobilka, B. (2007) Structure and conformational changes in the C-terminal domain of the $\beta$32-adrenoceptor: Insights from fluoresence resonance energy transfer studies. *J. Biol. Chem. 282*, 13895−13905.
(42) Shoichet, B. K., and Kobilka, B. K. (2012) Structure-based drug screening for G-protein-coupled receptors. *Trends Pharmacol. Sci. 33*, 268−272.
(43) Bockenhauer, S., Fürstenberg, A., Yao, X. J., Kobilka, B. K., and Moerner, W. E. (2011) Conformational dynamics of single G protein-coupled receptors in solution. *J. Phys. Chem. B 115*, 13328−13338.
(44) Bruno, A., Guadix, A. E., and Costantino, G. (2009) Molecular dynamics simulation of the heterodimeric mglur2/5ht2a complex. An atomistic resolution study of a potential new target in psychiatric conditions. *J. Chem. Inf. Model. 49*, 1602−1616.
(45) Filizola, M., Wang, S., and Weinstein, H. (2006) Dynamic models of G-protein coupled receptor dimers: Indications of asymmetry in the rhodopsin dimer from molecular dynamics simulations in a POPC bilayer. *J. Comput.-Aided Mol. Des. 20*, 405−416.
(46) Grossfield, A. (2011) Recent progress in the study of G protein-coupled receptors with molecular dynamics computer simulations. *Biochim. Biophys. Acta 1808*, 1868−1878.
(47) Hallmen, C., and Wiese, M. (2006) Molecular dynamics simulation of the human adenosine A3 receptor: Agonist induced conformational changes of Trp243. *J. Comput.-Aided Mol. Des. 20*, 673−684.
(48) Hoffert, J. D., Pisitkun, T., Saeed, F., Song, J. H., Chou, C.-L., and Knepper, M. A. (2012) Dynamics of the G protein-coupled vasopressin V2 receptor signaling network revealed by quantitative phosphoproteomics. *Mol. Cell. Proteomics 11*, M111.014613.
(49) Kimura, S. R., Tebben, A. J., and Langley, D. R. (2008) Expanding GPCR homology model binding sites via a balloon potential: A molecular dynamics refinement approach. *Proteins: Struct., Funct., Bioinf. 71*, 1919−1929.
(50) Simpson, L. M., Wall, I. D., Blaney, F. E., and Reynolds, C. A. (2011) Modeling GPCR active state conformations: The $\beta$2-adrenergic receptor. *Proteins: Struct., Funct., Bioinf. 79*, 1441−1457.
(51) Jojart, B., Kiss, R., Viskolcz, B., and Keseru, G. M. (2008) Activation mechanism of the human histamine H4 receptor; An explicit membrane molecular dynamics simulation study. *J. Chem. Inf. Model. 48*, 1199−1210.
(52) Miao, Y., Nichols, S. E., Gasper, P. M., Metzger, V. T., and McCammon, J. A. (2013) Activation and dynamic network of the M2 muscarinic receptor. *Proc. Natl. Acad. Sci. U.S.A. 110*, 10982−10987.
(53) Perilla, J. R., Beckstein, O., Denning, E. J., and Woolf, T. B. (2010) Computing ensembles of transitions from stable states: Dynamics importance sampling. *J. Comput. Chem. 32*, 196−209.
(54) Bettinelli, I., Graziani, D., Marconi, C., Pedretti, A., and Vistoli, G. (2011) The approach of conformational chimeras to model the role of proline-containing helices on GPCR mobility: The fertile case of cys-LTR1. *ChemMedChem 6*, 1217−1227.
(55) Gao, Q.-B., and Wang, Z.-Z. (2006) Classification of G-protein coupled receptors at four levels. *Protein Eng., Des. Sel. 19*, 511−516.
(56) Gloriam, D. E., Foord, S. M., Blaney, F. E., and Garland, S. L. (2009) Definition of the G protein-coupled receptor transmembrane bundle binding pocket and calculation of receptor similarities for drug design. *J. Med. Chem. 52*, 4429−4442.
(57) Hall, S. E., Roberts, K., and Vaidehi, N. (2009) Position of helical kinks in membrane protein crystal structures and the accuracy of computational prediction. *J. Mol. Graphics Modell. 27*, 944−950.
(58) Langelaan, D. N., Wieczorek, M., Blouin, C., and Rainey, J. K. (2010) improved helix and kink characterization in membrane proteins allows evaluation of kink sequence predictors. *J. Chem. Inf. Model. 50*, 2213−2220.
(59) Wistrand, M., Käll, L., and Sonnhammer, E. L. L. (2006) A general model of G protein-coupled receptor sequences and its application to detect remote homologs. *Protein Sci. 15*, 509−521.
(60) Yohannan, S., Faham, S., Yang, D., Whitelegge, J. P., and Bowie, J. U. (2004) The evolution of transmembrane helix kinks and the structural diversity of G protein-coupled receptors. *Proc. Natl. Acad. Sci. U.S.A. 101*, 959−963.
(61) Venkatakrishnan, A. J., Deupi, X., Lebon, G., Tate, C. G., Schertler, G. F., and Babu, M. M. (2013) Molecular signatures of G-protein-coupled receptors. *Nature 494*, 185−194.
(62) Heifetz, A., Morris, G. B., Biggin, P. C., Barker, O., Fryatt, T., Bentley, J., Hallett, D., Manikowski, D., Pal, S., Reifegerste, R., Slack, M., and Law, R. (2012) Study of human Orexin-1 and -2 -G-protein-coupled receptors with novel and published antagonists by modeling, molecular dynamics simulations, and site-directed mutagenesis. *Biochemistry 51*, 3178−3197.
(63) Palczewski, K., Kumasaka, T., Hori, T., Behnke, C. A., Motoshima, H., Fox, B. A., Le Trong, I., Teller, D. C., Okada, T., Stenkamp, R. E., Yamamoto, M., and Miyano, M. (2000) Crystal structure of rhodopsin: A G protein-coupled receptor. *Science 289*, 739−745.
(64) Chien, E. Y. T., Liu, W., Zhao, Q., Katritch, V., Won Han, G., Hanson, M. A., Shi, L., Newman, A. H., Javitch, J. A., Cherezov, V., and Stevens, R. C. (2010) Structure of the human dopamine D3 receptor in complex with a D2/D3 selective antagonist. *Science 330*, 1091−1095.
(65) Jaakola, V.-P., and Ijzerman, A. P. (2010) The crystallographic structure of the human adenosine A2A receptor in a high-affinity antagonist-bound state: Implications for GPCR drug screening and design. *Curr. Opin. Struct. Biol. 20*, 401−414.
(66) Cherezov, V., Rosenbaum, D. M., Hanson, M. A., Rasmussen, S. G. F., Thian, F. S., Kobilka, T. S., Choi, H.-J., Kuhn, P., Weis, W. I., Kobilka, B. K., and Stevens, R. C. (2007) High-resolution crystal structure of an engineered human $\beta$2-adrenergic G protein-coupled receptor. *Science 318*, 1258−1265.
(67) Courcot, B., and Bridgeman, A. J. (2011) Modeling the interactions between polyoxometalates and their environment. *J. Comput. Chem. 32*, 3143−3153.
(68) Wolf, M. G., Hoefling, M., Aponte-Santamaría, C., Grubmüller, H., and Groenhof, G. (2010) g_membed: Efficient insertion of a membrane protein into an equilibrated lipid bilayer with minimal perturbation. *J. Comput. Chem. 31*, 2169−2174.
(69) Hess, B., Kutzner, C., van der Spoel, D., and Lindahl, E. (2008) GROMACS 4: Algorithms for highly efficient, load-balanced, and scalable molecular simuation. *J. Chem. Theory Comput. 4*, 435−447.
(70) Jorgensen, W. L., Maxwell, D. S., and Tirado-Rives, J. (1996) Development and testing of the OPLS all-atom force field on conformational energetics and properties of organic liquids. *J. Am. Chem. Soc. 118*, 11225−11236.
(71) Kaminski, G. A., Friesner, R. A., Tirado-Rives, J., and Jorgensen, W. L. (2001) Evaluation and Reparametrization of the OPLS-AA Force Field for Proteins via Comparison with Accurate Quantum Chemical Calculations on Peptides. *J. Phys. Chem. B 105*, 6474−6487.
(72) Jorgensen, W. L., Chandresekhar, J., Madura, J. D., Impey, R. W., and Klein, M. L. (1983) Comparison of simple potential functions for simulating liquid water. *J. Chem. Phys. 79*, 926−935.
(73) Van Gunsteren, W. F., and Berendsen, H. J. C. (1988) A leap-frog algorithm for stochastic dynamics. *Mol. Simul. 1*, 173−185.

(74) Essman, U., Perera, L., Berkowitz, M. L., Darden, T., Lee, H., and Pedersen, L. G. (1995) A smooth particle mesh Ewald method. *J. Chem. Phys. 103*, 8577−8593.
(75) Hess, B., Bekker, J., Berendsen, H. J. C., and Fraaije, J. G. E. M. (1997) LINCS: A linear constraint solver for molecular simulations. *J. Comput. Chem. 18*, 1463−1472.
(76) Korb, O., Olsson, T. S. G., Bowden, S. J., Hall, R. J., Verdonk, M. L., Liebeschuetz, J. W., and Cole, J. C. (2012) Potential and limitations of ensemble docking. *J. Chem. Inf. Model. 52*, 1262−1274.
(77) Liebeschuetz, J., Cole, J., and Korb, O. (2012) Pose prediction and virtual screening performance of GOLD scoring functions in a standardized test. *J. Comput.-Aided Mol. Des. 26*, 737−748.
(78) Feldman, H. J., and Labute, P. (2010) Pocket similarity: Are $\alpha$ carbons enough? *J. Chem. Inf. Model. 50*, 1466−1475.
(79) Madabushi, S., Gross, A. K., Philippi, A., Meng, E. C., Wensel, T. G., and Lichtarge, O. (2004) Evolutionary trace of G protein-coupled receptors reveals clusters of residues that determine global and class-specific functions. *J. Biol. Chem. 279*, 8126−8132.
(80) Rodriguez, D., Pineiro, A., and Gutirrez-de-Teran, H. (2011) Molecular dynamics simulations reveal insights into key structural elements of adenosine receptors. *Biochemistry 50*, 4194−4208.
(81) Thepchatri, P., Eliseo, T., Cicero, D. O., Myles, D., and Snyder, J. P. (2007) Relationship among ligand conformations in solution, in the solid state, and at the HSP90 binding site: Geldanamycin and radicicol. *J. Am. Chem. Soc. 129*, 3127−3134.
(82) Hascall, T., Baik, M. H., Bridgewater, B. M., Shin, J. H., Churchill, D. G., Friesner, R. A., and Parkin, G. (2002) A non-classical hydrogen bond in the molybdenum arene complex [$\eta$6-$C_6H_5C_6H_3$(Ph)OH]Mo($PMe_3$)$_3$: Evidence that hydrogen bonding facilitates oxidative addition of the O-H bond. *Chem. Commun. 21*, 2644−2645.
(83) Mohamed, M. N. A., Watts, H. D., Guo, J., Catchmark, J. M., and Kubicki, J. D. (2010) MP2, density functional theory, and molecular mechanical calculations of C−H···$\pi$ and hydrogen bond interactions in a cellulose-binding module−cellulose model system. *Carbohydr. Res. 345*, 1741−1751.
(84) Trzaskowski, B., Latek, D., Yuan, S., Ghoshdastider, U., Debinski, A., and Filipek, S. (2012) Action of molecular switches in GPCRs: Theoretical and experimental studies. *Curr. Med. Chem. 19*, 1090−1109.
(85) Kneissl, B., Mueller, S. C., Tautermann, C. S., and Hildebrandt, A. (2011) String kernels and high-quality data set for improved prediction of kinked helices in $\alpha$-helical membrane proteins. *J. Chem. Inf. Model. 51*, 3017−3025.
(86) Abrol, R., Kim, S.-K., Bray, J. K., Trzaskowski, B., and Goddard, W. A., III (2013) Chapter two: Conformational ensemble view of G protein-coupled receptors and the effect of mutations and ligand binding. In *Methods in Enzymology* (Conn, P. M., Ed.) pp 31−48, Academic Press, New York.
(87) Tate, C. G. (2012) A crystal clear solution for determining G-protein-coupled receptor structures. *Trends Biochem. Sci. 37*, 343−352.